



ELSEVIER



BASIC SCIENCE

Nanomedicine: Nanotechnology, Biology, and Medicine
43 (2022) 102556



nanomedjournal.com

Feature Article

Optical detection of atherosclerosis at molecular level by optical coherence tomography: An in vitro study

Tamara Muñoz-Ortiz, MSc^{a,b}, Jie Hu, PhD^c, Francisco Sanz-Rodríguez, PhD^d,
Dirk H. Orgtjes, PhD^{a,e}, Daniel Jaque, PhD^{a,b,e}, Diego Méndez-González, PhD^{a,e},
Río Aguilar, MD, PhD^f, Fernando Alfonso, MD, PhD^f, Fernando Rivero, MD^f,
Emma Martín Rodríguez, PhD^{b,e,g,*}, José García Solé, PhD^{a,b}

^aNanomaterials for Bioimaging Group (nanoBIG), Departamento de Física de Materiales, Facultad de Ciencias, Universidad Autónoma de Madrid, Madrid, Spain

^bInstituto Nicolás Cabrera, Facultad de Ciencias, Universidad Autónoma de Madrid, Madrid, Spain

^cXiamen Institute of Rare-earth Materials, Haixi Institutes Chinese Academy of Sciences, Xiamen, Fujian, China

^dNanomaterials for Bioimaging Group (nanoBIG), Departamento de Biología, Facultad de Ciencias, Universidad Autónoma de Madrid, Madrid, Spain

^eNanomaterials for Bioimaging Group (nanoBIG), Instituto Ramón y Cajal de Investigación, Sanitaria Hospital Ramón y Cajal, Madrid, Spain

^fCardiology Department, Hospital Universitario de la Princesa, Instituto Investigación Sanitaria Princesa (IIS-IP), CIBER-CV, Universidad Autónoma de Madrid, Madrid, Spain.

^gNanomaterials for Bioimaging Group (nanoBIG), Departamento de Física Aplicada, Facultad de Ciencias, Universidad Autónoma de Madrid, Madrid, Spain

Revised 22 February 2022

Abstract

There is an urgent need for contrast agents to detect the first inflammation stage of atherosclerosis by cardiovascular optical coherence tomography (CV-OCT), the imaging technique with the highest spatial resolution and sensitivity of those used during coronary interventions. Gold nanoshells (GNSs) provide the strongest signal by CV-OCT. GNSs are functionalized with the cLABL peptide that binds specifically to the ICAM-1 molecule upregulated in the first stage of atherosclerosis. Dark field microscopy and CV-OCT are used to evaluate the specific adhesion of these functionalized GNSs to activated endothelial cells. This adhesion is investigated under static and dynamic conditions, for shear stresses comparable to those of physiological conditions. An increase in the scattering signal given by the functionalized GNSs attached to activated cells is observed compared to non-activated cells. Thus, cLABL-functionalized GNSs behave as excellent contrast agents for CV-OCT and promise a novel strategy for clinical molecular imaging of atherosclerosis.

© 2022 The Authors. Published by Elsevier Inc. This is an open access article under the CC BY license (<http://creativecommons.org/licenses/by/4.0/>).

Key words: Gold nanoshells; Cardiovascular imaging; Optical coherence tomography; Molecular imaging

Nowadays, cardiovascular diseases are the main cause of mortality in the developed world. It is also expected that these diseases will remain the first cause of death globally for the next decade.¹ This has incentivized the scientific community to con-

sider new strategies for the prediction, prevention and treatment of atherosclerosis, including those based on the novel discipline of nanomedicine.^{2–6} Atherosclerosis consists of a progressive inflammatory process characterized by a gradual thickening of the

Abbreviations: OCT, Optical Coherence Tomography; CV-OCT, Cardiovascular Optical Coherence Tomography; cLABL, PenITDGEATDSGC peptide; DFM, Dark Field Microscopy; GNSs, Gold Nanoshells.

Funding: Ministerio de Ciencia e Innovación (PID2019-106211RB-I00); Instituto de Salud Carlos III (PI16/00812) and (PI19/00565); Comunidad Autónoma de Madrid (S2017/BMD-3867 RENIM-CM) co-financed by the European Structural and Investment Fund; Horizon 2020 FET Open grant agreement no. 801305 (NanoTBTech project); Fundación para la Investigación Biomédica del Hospital Universitario Ramón y Cajal project IMP18_38 (2018/0265); COST action CA1740; Chinese Academy of Sciences Pioneer “Hundred Talents Program” Young talents (Class C) (JH).

* Corresponding author.

E-mail address: emma.martin@uam.es (E. Martín Rodríguez).

<https://doi.org/10.1016/j.nano.2022.102556>

1549-9634/© 2022 The Authors. Published by Elsevier Inc. This is an open access article under the CC BY license (<http://creativecommons.org/licenses/by/4.0/>)

Please cite this article as: Muñoz-Ortiz T, et al, Optical detection of atherosclerosis at molecular level by optical coherence tomography: An in vitro study. *Nanomedicine: NBM* 2022;43:102556, <https://doi.org/10.1016/j.nano.2022.102556>

artery walls, leading to the formation of atherosclerotic plaques in the coronary walls. Atherosclerotic plaques reduce blood flow and so, the amount of oxygen and other nutrients reaching the different parts of the body. The gradual thickening of artery walls is a silent process, so symptoms appear late, when the lumen is too narrow or, suddenly, when plaque rupture occurs and evolves into thrombosis. Thus, there is an increasing interest in detecting the early and pre-symptomatic stages in the development of atherosclerotic plaques when the lumen has not been narrowed yet. The detection of the responsible biological processes at the cellular or molecular level using molecular imaging is of particular interest. This imaging modality relies on the use of suitable contrast agents to specifically recognize cellular or subcellular targets that indicate the development of atherosclerosis. Although several experimental techniques have been used to characterize these atherosclerotic stages, of importance are those used in patients during diagnostic and interventional coronary procedures, since they provide a unique opportunity for in situ diagnosis and prognostic assessment. During these clinical procedures, cardiologists use four main imaging techniques: X-ray, ultrasound, angiography, and optical coherence tomography (OCT). Among them, OCT is the diagnostic clinical tool with the highest spatial resolution: in the order of 10 μm . Thus, despite its limited depth penetration (few mm), cardiovascular optical coherence tomography (CV-OCT) is nowadays widely used during catheterization procedures for evaluating the superficial plaque morphology at a micrometric scale.^{7,8} OCT displays also a very high sensitivity, higher than 100 dB, and is, therefore, able to detect changes in tissue-related reflectivity as low as 10^{-10} .^{9,10} This aspect is of great relevance because many targets of interest associated with the first inflammation stages are present at very low (nanomolar) concentrations. However, obtaining details at the cellular or molecular level by CV-OCT requires the use of suitable contrast agents providing contrast at the OCT operating wavelengths (around 1300 nm in modern CV-OCT systems). In this respect, several contrast agents for CV-OCT have been developed, including microbubbles, iron oxide microparticles and, more recently, gold nanoparticles.^{2,3,11–14} Nevertheless, most of these agents do not provide images of processes at the subcellular level, and so real molecular imaging.

In this sense, systematic studies have recently demonstrated that gold nanoparticles of different morphologies (shapes, composition and dimensions) display broad plasmonic extinction bands in the near-infrared spectral region and, more importantly, provide a high backscattering signal at the CV-OCT working wavelength.^{15–17} In addition, the gold surface of these nanoparticles makes them biologically inert and highly biocompatible, making conjugation to proteins for in vivo applications possible. Consequently, gold nanoparticles emerge as excellent nano-contrast agents for cardiovascular OCT. Recently our group determined that core/shell plasmonic nanoparticles, consisting of a SiO_2 core (of about 200 nm) surrounded by thin shell of gold (of about 15 nm), produce the largest scattering cross-section (about $5 \times 10^{-10} \text{ cm}^2$) at the CV-OCT wavelength and therefore the highest contrast in cardiovascular interventional devices.¹⁵ Gold nanoshells (GNSs) have been also successfully used for enhanced cell imaging by CV-OCT.¹⁸ Thus, these GNSs appear as the most suitable nanoparticles for molecular

imaging of atherosclerosis by CV-OCT, and particularly for detecting the earliest stages of this disease, where the other interventional techniques are yet blind. However, for this purpose these nanoparticles must be properly functionalized with molecules or antibodies that can recognize the specific receptors that are upregulated in the artery walls at the first stages of atherosclerosis development.

In 2008, J. Sanz and Z. A. Fayad classified the progressive stages of the development of an atherosclerotic lesion by six stages: from a normal vessel to a vessel with a well-developed atheroma (stage 6).^{4,19} Importantly, they also determined the main potential molecular targets associated to each one of these stages. Each stage displays different cellular inflammatory and molecular processes, which finally build up a plaque, eventually leading to a substantial narrowing of the arteries.²⁰ The earliest stage of atherosclerosis (stage 1) begins when low-density lipoproteins (LDLs), i.e. cholesterol-rich lipo-proteic particles, cross a damaged endothelium and suffer chemical modifications (oxidation) that trigger the inflammatory response of the tissue.²¹ This stage is accompanied by the overexpression of several adhesion molecules, such as vascular cell adhesion molecule 1 (VCAM-1), intercellular adhesion molecule 1 (ICAM-1) as well as P and E selectins.^{2,22–24} Consequently, nanoparticles designed to diagnose this stage must be properly functionalized with ligands and/or antibodies capable of targeting the above-mentioned up-regulated molecules. The ICAM-1 molecule is part of the immune response (inflammation), and its activation and increased expression allow leukocytes to bind to the endothelial cells via the leukocyte function-associated antigen-1 (LFA-1).²⁵ Therefore, an LFA-1 protein coating could be used to bind nanoparticles to cells overexpressing high levels of ICAM-1 on the surface. However, large proteins or antibodies for targeting have some general limitations, like the prize to obtain pure materials and the difficulty in maintaining the structural and functional stability. Hence, one of the principal efforts in the pharmaceutical industry is the development of small peptide inhibitors for a given target receptor. In this respect, the cyclo^{1,12} PenITDGEATDSGC peptide (abbreviated cLABEL), a synthetic binding peptide sequence obtained from the I-domain of the α -subunit of LFA-1, has been previously demonstrated to possess high avidity for ICAM-1 receptors overexpressed on the cell surface.^{26,27} This makes this small peptide an ideal candidate for the targeting of ICAM-1 by gold nanoshells.

In this work, we establish a systematic prospective protocol to investigate the in vitro specific adhesion efficiency of cLABEL-functionalized GNSs to inflamed endothelial cells. For this purpose, we first employed dark field microscopy (DFM) to determine the scattered signal given by GNSs under both static and dynamic conditions. These results were then corroborated by CV-OCT, proving that functionalized GNSs are very promising contrast agents to detect incipient atherosclerosis during clinical catheterization procedures.

Methods

Details about the surface modification of the GNSs, and the cell culture and cytotoxicity protocols can be found in the Supplementary Materials section.

Extinction spectra

Extinction spectra of the different GNSs colloidal dispersions were all measured at room temperature with a Perkin Elmer Lambda 1050 spectrophotometer, covering a spectral range from 400 to 1380 nm.

Fourier transform infrared spectroscopy (FTIR)

To demonstrate the successful functionalization of GNSs with the cLABL peptide, FTIR was used. Spectra were measured using the transmission mode on a IRSpirit-T instrument (SHIMADZU), performing 128 scans in the 400–4000 cm^{-1} range with 4 cm^{-1} resolution. The samples were prepared forming KBr pellets containing 1 wt% of the analyzed material.

Dynamic light scattering (DLS)

Experimental Details. The hydrodynamic diameter of the GNSs was determined by DLS. For this purpose, we used a Malvern Zetasizer Nano ZS90 (Malvern) equipment and size distribution was measured at 20 °C with an equilibration time of 60 s and a detection angle of 173° (backscattering).

GNSs-cell specific adhesion experiments

Incubations of GNSs (functionalized and non-functionalized) were carried out to estimate the GNSs-cell adhesion efficiency. These incubations were performed under static and dynamic (flow) conditions of the GNSs dispersions.

(i) Static experiments

HMEC cells were incubated for 1 h at 37 °C with GNSs in PBS dispersions (cLABL-functionalized and non-functionalized, as control). After incubation, the successful adhesion of GNSs to HMEC cells was investigated by both dark field microscopy (DFM) and CV-OCT.

For DFM imaging, a Nikon Eclipse Ti2-U microscope was employed. The DFM condenser has a numerical aperture of 0.80–0.95, and a 40× microscope objective (Nikon) with a numerical aperture of 0.65 was used. The sample was illuminated with a broadband white LED source and images were taken with a visible CMOS camera (UEye, Thorlabs).

For OCT imaging, we used a clinical CV-OCT system commercially available (St. Jude Medical with Dragonfly OPTIS™ Imaging Catheter, Abbott). This interferometric system works in the frequency domain with a super-luminescent diode emitting infrared light centered at 1320 nm with a bandwidth of 200 nm. The axial resolution of this CV-OCT system is 15 μm , with a tissue penetration depth as large as 3 mm.

(ii) Dynamic experiments

Adhesion experiments of the GNSs to the HMEC cells were also carried out under two different shear stresses of the flowing GNSs. For this purpose, 40 mm^2 cell culture coverslips were mounted on a parallel-plate flow chamber (Warner Instruments, RC-30WA) connected to a syringe pump (New Era NE-300 Just Infusion™) that can provide constant flow rates up to a maxi-

mum value of about 4 dyn cm^{-2} . The procedure in this case is as follows: First, cells were TNF- α activated to overexpress ICAM-1. Then, the different dispersions of GNSs (functionalized and non-functionalized), with a fixed gold concentration of 5 $\mu\text{g mL}^{-1}$, were made to flow over the activated cells for 5 min at each shear stress. After that, the cells are washed with PBS for 1 additional minute. Images were obtained by DFM every minute during the circulation time, to compare the corresponding light scattered signals and evaluate the GNSs-cell adhesion efficiency for each condition. Shear stress magnitudes were calculated from the established flow rates given by Eq. [2]²⁸:

$$\tau_w = \frac{6Q}{bh^2} \quad (2)$$

where τ_w is the wall shear stress, μ the apparent fluid viscosity (we took that of water at 37 °C; 0.0076 P), Q is the flow rate, b is the gasket width and h the gasket thickness.

Image processing

GNSs have an intense plasmon resonance at 700 nm (Figure 2, A), for this reason, in the raw DFM images the nanoparticles appear as reddish dots. Thus, a color-filter was applied to the raw images (using a custom MATLAB code) to discriminate the contribution of the GNSs from the whole scattering signal. Then the intensity due to nanoparticles attached to cells of the color-filtered images was determined using ImageJ software.

Results and discussion

The authors have previously studied a variety of gold nanoparticles of different morphologies, shapes, and sizes, demonstrating that those made of a silica core of 200 nm and a gold shell of 15 nm thickness (called gold nanoshells, GNSs) provide the highest backscattering at 1320 nm, i.e., at the CV-OCT working wavelength.¹⁵ Thus, these GNSs are the contrast agents used all along this work.

To compare between passive and active cell targeting of HMEC cells, two different surface coatings for the GNSs (contrast agents) were used:

- (i) GNSs coated with polyethylene glycol (labeled as GNSs@PEG), for passive targeting (or control), as this coating does not provide specific particle-cell interactions while assuring aqueous stability.
- (ii) GNSs coated with the cLABL peptide, for active targeting of the ICAM-1 molecules that are upregulated after TNF- α activation (labeled as GNSs@iCAM). A simplified scheme of a GNS decorated with the peptide is shown in Figure 1, A.

In Figure 1, B we have included the dynamic light scattering (DLS) size distribution obtained for the non-functionalized (GNSs@PEG) and functionalized (GNSs@iCAM) nanoparticles. It can be seen how the functionalization with the peptide yields GNSs with a 31% higher hydrodynamic diameter, compared with non-functionalized GNSs. Figure 1, C shows the FTIR spectra of functionalized and non-functionalized GNSs together with that of the cLABL peptide alone. Additional

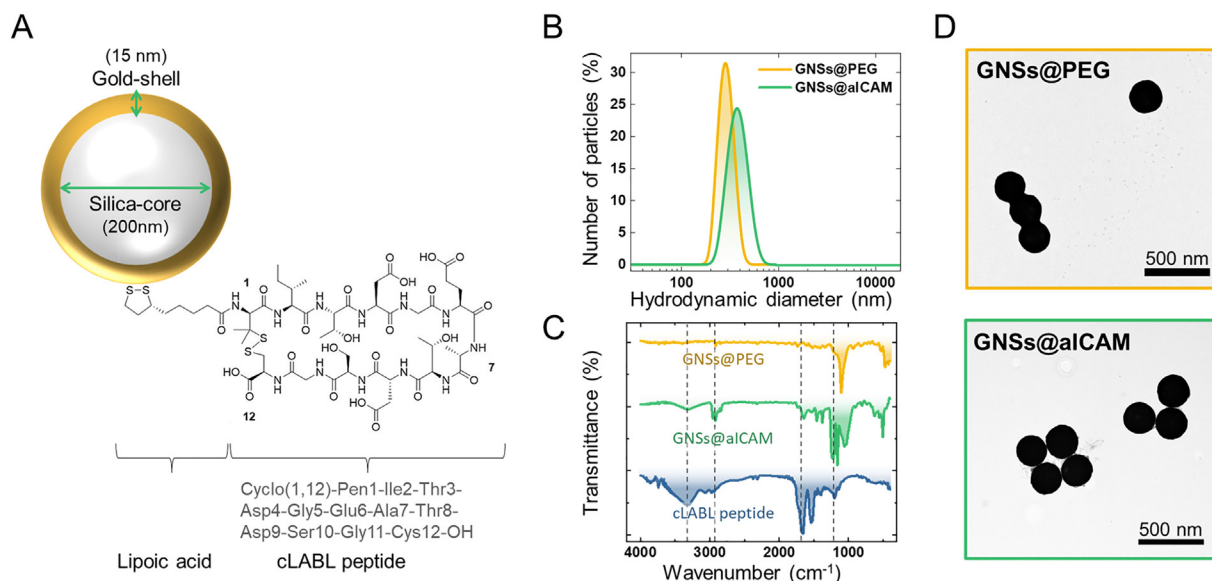


Figure 1. (A) GNSs@alCAM schematic drawing. (B) Hydrodynamic diameter of GNSs@PEG and GNSs@alCAM. (C) FTIR spectra of GNSs@PEG, GNSs@alCAM, and cLABL peptide. (D) TEM images of GNSs@PEG (top) and GNSs@alCAM (bottom).

vibrational bands are found in the GNSs@alCAM FTIR spectrum (see dashed lines) compared to the GNSs@PEG spectrum. More specifically, the broad band at 3300 cm^{-1} can be assigned to O-H and N-H vibrations, additional vibrations from the hydrocarbon skeleton of the amino acid residues correspond to the bands at around 2900 and 1200 cm^{-1} , and the increased presence of carboxylates and amides results in an increase in the C=O stretching vibration at around 1650 cm^{-1} . These bands are all characteristic of the cLABL peptide, as shown in Figure 1, C. This demonstrates the successful functionalization of our GNSs with the cLABL peptide. The transmission electron microscopy (TEM) images of the GNSs (Figure 1, D), together with the size

distribution given by DLS (Figure 1, B), indicate that no significant GNSs aggregation takes place during the surface modification process. Nevertheless, to confirm the water colloidal stability and so the absence of aggregates of functionalized particles, ζ -potential measurements were also performed (Figure S1 of the supplementary material). These results show that all the aqueous dispersions used in this work (with ζ -potential around -32 mV) are all colloidal stable.

The normalized extinction spectra of biocompatible phosphate-buffered saline (PBS) colloidal dispersions containing the above-mentioned GNSs are shown in Figure 2, A. Due to their core-shell structure, the spectra of GNSs consist of broad

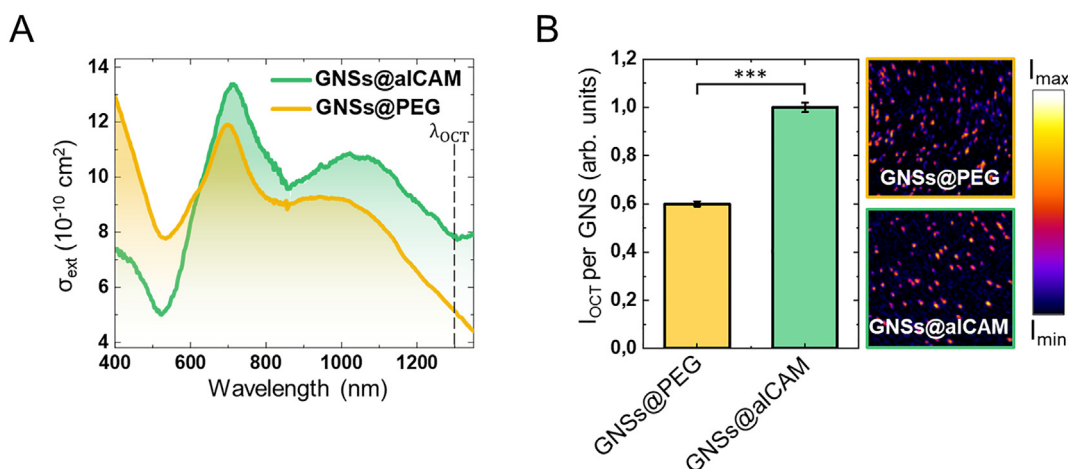


Figure 2. (A) Extinction spectrum of GNSs functionalized (GNSs@alCAM) and PEG-coated (GNSs@PEG). Dashed line indicates the working wavelength of the cardiovascular OCT system (1325 nm). (B) OCT intensity per nanoparticle signal (left) given by both GNSs and comparative OCT cross-sectional images (right). The statistical difference is determined by the two-sample t test ($***P \leq .001$).

extinction bands with two main surface plasmon resonances, peaking at about 700 nm and 1000 nm, respectively. Importantly, both (functionalized and non-functionalized) GNSs show a relevant extinction coefficient at 1320 nm, i.e., at the CV-OCT working wavelength (see dashed line). Interestingly, anti-ICAM-1 coating provides the GNSs with about 60% higher extinction coefficient at 1320 nm than the PEG-coated GNSs. Although the origin of this extinction enhancement is not completely understood at this point, we state that it is mostly due to an expected larger Rayleigh scattering increase due to the hydrodynamic diameter increase after the GNSs surface decoration with cLABL peptide. In fact, to further assess this increased scattering effect, the OCT backscattered intensity per particle was estimated for both GNSs@PEG and GNSs@aICAM, after averaging from several OCT cross-sectional images like the ones provided in Figure 2, B. The results show that the OCT backscattering intensity increases by 66% for the GNSs@aICAM compared to the GNSs@PEG, in good agreement with the observed increase in the extinction cross-section.

The next step to investigate the adhesion efficiency of the GNSs is to test the effectiveness of TNF- α stimulation of the endothelial HMEC cells to trigger the overexpression of ICAM-1 molecules. For this purpose, we carried out flow cytometry experiments. Figure 3 shows the results obtained for basal and TNF- α activated cell cultures, together with a control in which the basal cells were not incubated with ICAM-1 antibody. Comparing the total fluorescence intensity collected in the FL-1 channel one can see that the fluorescence intensity increases by about one order of magnitude for the activated cells compared to the basal cells. Thus, we conclude that TNF- α activation does effectively lead to a substantial increase of ICAM-1 expression in the HMEC cells. It is also noteworthy that, even if the number of molecules expressed by activated cells is much higher than in the basal cells, the later also express this protein, since the fluorescence intensity increases compared to the control situation.

Once it was demonstrated that HMEC activated cells overexpress a substantial number of ICAM-1 molecules in compar-

ison with the basal (non-activated) cells, we incubated both kinds of cells with dispersions of GNSs (functionalized and non-functionalized) in PBS for 1 h at 37 °C. The gold mass concentration chosen for the dispersions is 5 $\mu\text{g mL}^{-1}$; at this concentration both the functionalized and non-functionalized nanoparticles do not provide cytotoxic effects (see Figure S2 in the supplementary material section). Moreover, it should be noticed that the cell viability remains as good as 80% for much higher concentrations (15 $\mu\text{g mL}^{-1}$), which could be required for future in vivo experiments to provide enough scattering contrast when working at very short cell-nanoparticle interaction times. Dark field microscopy (DFM) was first used to compare the GNSs-cell binding affinity in static conditions between functionalized and non-functionalized GNSs, to discriminate between active and passive targeting. Figure 4, A shows four representative DFM images of endothelial cells layers in the basal and TNF- α stimulated states after incubation with two different GNSs colloidal dispersions: one with GNSs@PEG for passive targeting, and the other one with GNSs@aICAM for active targeting. The GNSs appear in the DFM images as red spots due to their plasmon resonance peaking at 700 nm. For cells incubated with GNSs@PEG (non-functionalized nanoparticles) the number of red spots found in the images is similar for both basal and activated states. On the other hand, the use of GNSs@aICAM (functionalized nanoparticles) in the incubation procedure leads to an increase in the number of GNSs attached to the cells for both basal and activated cells.

The GNSs-cell binding affinity can be quantified following the image processing procedure described in the Methods section. Briefly, images are color-filtered so that only the intensity due to the reddish pixels (i.e., the intensity due to GNSs) is registered. Results obtained after averaging over several cells are shown in Figure 4, B. For cells incubated with non-functionalized GNSs, the mean intensity is low (about 0.2) and similar for basal and activated cells, revealing a certain amount of passive targeting. Incubation with functionalized GNSs produces an intensity increase from 0.2 to about 0.75 for the basal state cells, while an additional increase up to 1 is observed for cells in the

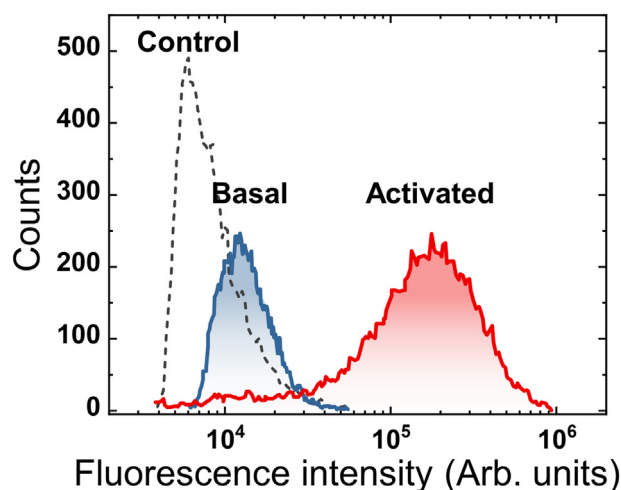


Figure 3. Flow cytometry data of the expression of ICAM-1 before (basal, blue spectrum) and after (activated, red spectrum) TNF- α activation of HMEC cells. The control case (basal cells not incubated with the ICAM-1 antibody) is included in dashed line.

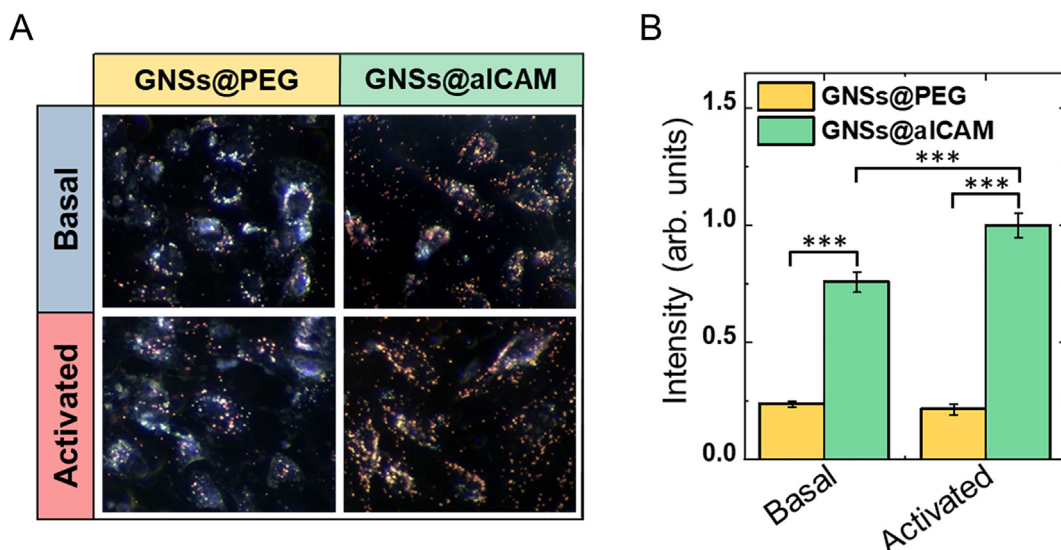


Figure 4. (A) Dark field microscopy images of basal and activated HMEC cells incubated with GNSs@PEG or GNSs@aICAM. (B) Average total intensity per cell for both basal and activated cells. Statistical difference is determined by the two-sample *t* test (***) $P \leq .001$.

activated state. We defined the specific adhesion efficiency as the relative change in the intensity of the images of cells incubated with GNSs@aICAM in the activated state (Eq. [1]).

$$\eta = \frac{I_{aICAM}^{act} - I_{aICAM}^{bas}}{I_{aICAM}^{act}} \quad (1)$$

Where I_{aICAM}^{act} and I_{aICAM}^{bas} are the mean intensity scattered by the cells after the color-filtration (i.e., the intensity due to GNSs) for activated and basal cultures, respectively, after incubation with GNSs@aICAM. Thus, this efficiency indicates the ability of the functionalized nanoparticles to detect the overexpression of ICAM-1 molecules because of TNF- α activation, i.e., after the cell inflammation occurring in the first stage of atherosclerosis development. From Figure 4, B, it can be estimated that the specific adhesion efficiency in static conditions is close to 23%, proving that active-targeting of the ICAM-1 molecules is taking place.

We then evaluated the suitability of the CV-OCT technique to detect the specific targeting of functionalized GNSs to the HMEC activated cells. For this purpose, the OCT catheter tip was placed under the endothelial cells culture dishes to obtain the OCT backscattering signals of these cell monolayers, using the pull-back function. It is important to mention here that the concentration used for the incubations ($5 \mu\text{g mL}^{-1}$) lies within the concentration range at which the OCT intensity responds linearly to the GNSs' concentration (see Figure S3 of the Supplementary material). Figure 5, A shows the OCT images of the basal and activated cell monolayers, after incubation with non-functionalized and functionalized GNSs. The bright areas are due to the backscattering produced by the cells and the GNSs bound to the cell culture. The OCT intensities (Figure 5, B) are calculated as the average of the total intensity of the bright pixels in all the frames of the pullback image. As was observed by DFM (see Figure 4, B), the OCT signal intensity obtained under passive targeting (using GNSs@

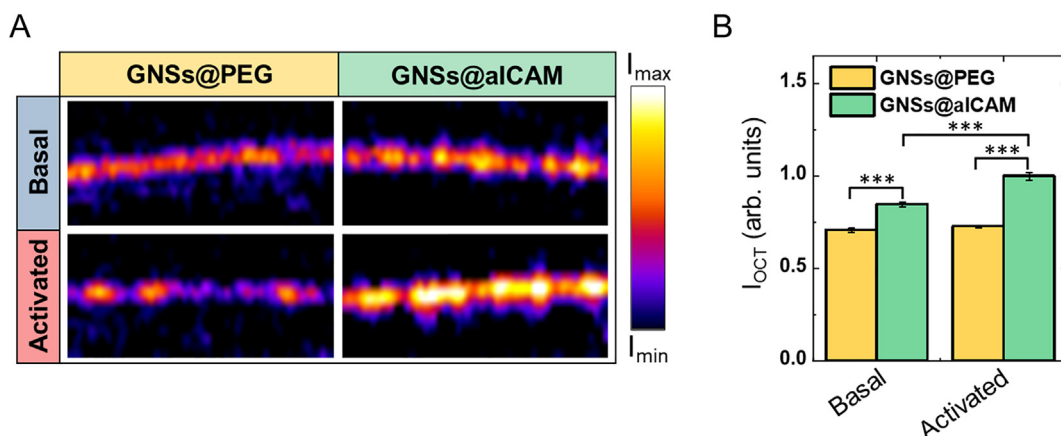


Figure 5. (A) OCT images of basal and activated HMEC cells monolayers incubated with GNSs@PEG or GNSs@aICAM. (B) OCT total intensity of the cell cultures areas for both basal and activated cells. Statistical difference is determined by the two-sample *t* test (***) $P \leq .001$.

PEG) is similar for the basal and activated states. Indeed, this result was expected due to the non-specific binding of these nanoparticles to the cells. However, for active targeting (using GNSs@aICAM) a measurable increase in the CV-OCT signal is detected for both the basal and activated states, revealing the ability of this technique to discriminate between active and passive targeting. The specific adhesion efficiency of this process has a value of about 17%, which is in good agreement with the efficiency obtained with DFM. Thus, this result clearly demonstrates the CV-OCT ability to discriminate between passive and active targeting and, more importantly, to detect the effect of TNF- α stimulation. In other words, this reveals the viability of GNSs@aICAM in combination with a clinical CV-OCT system to perform ICAM-1 molecular imaging.

Results included in Figures 4 and 5 have been obtained for static incubation conditions. Nevertheless, the potential of functionalized GNSs for molecular imaging of cardiovascular system requires measurements under flow conditions comparable to the ones that take place in the circulatory system. Figure 6 shows schematically how adhesion experiments under flow conditions were performed. Dispersions of GNSs with a gold mass concentration of $5 \mu\text{g mL}^{-1}$ were made to flow over cell monolayers in both basal and activated states at two different shear stresses, 1.7 and 3.5 dyn cm^{-2} . At these shear stresses, the GNS-cell interaction times (i.e., the time needed for the GNS to travel a distance equal to the cell length) are 3 ms and 1.5 ms respectively (see the Supplementary Material section for further details). For the sake of comparison, experiments were performed for both functionalized (GNSs@aICAM) and non-functionalized (GNSs@PEG) nanoparticles. DFM images were taken every minute for 5 min of circulation plus 1 min of PBS clearance. The specific adhesion efficiency was then determined.

Figure 7, A shows representative DFM images for different circulation times of functionalized and non-functionalized GNSs circulating over activated cells for a shear stress of 1.7 dyn cm^{-2} .

The number of red spots (i.e., those corresponding to GNSs) attached to the cells increases in the case of functionalized GNSs (see the white arrows in Figure 7, A), proving that it is possible to differentiate passive and active targeting even under dynamic conditions.

The color-filtered averaged intensity of all the cells for the different circulation times is calculated and corrected by the intensity at time 0. Results are provided in Figure 7, B, where the increment in DFM intensity is plotted as a function of the circulation time. For non-functionalized nanoparticles (GNSs@PEG), the DFM signal does not increase during the whole flow process, this fact revealing that there is not remarkable adhesion of nanoparticles. On the other hand, for the functionalized nanoparticles (GNSs@aICAM) the signal shows a linear increasing trend. This result indicates that the number of targeted GNSs bound to cells clearly increases with the circulating time.

For comparative purposes, a second set of DFM experiments was performed at larger shear stress, 3.5 dyn cm^{-2} , the highest value that can be achieved in our chamber. Figure 8 provides the averaged intensity increase (i.e., just due to GNSs) after all the dynamic process, obtained for the two shear stresses and all the possible combinations of cell states and GNSs.

Reference to Figure 8 shows that after TNF- α activation the number of functionalized (GNSs@aICAM) nanoparticles attached to the cells increases significantly in respect to the non-activated (basal) state. In fact, data given in Figure 8 at 6 min (after clearance) allow to determine how the specific adhesion efficiency (given by Eq. [1]) evolves when increasing the shear stress. The efficiencies obtained are 64% for 1.7 dyn cm^{-2} and 37% for 3.5 dyn cm^{-2} , meaning that a two-times increase of the shear stress leads to a dramatic reduction in the specific adhesion efficiency of the GNSs to the activated HMEC cells.

In comparison to the previous efficiency values obtained under dynamic conditions, one can clearly see that the efficiency obtained under static incubation (1 h) is certainly low (20%). This

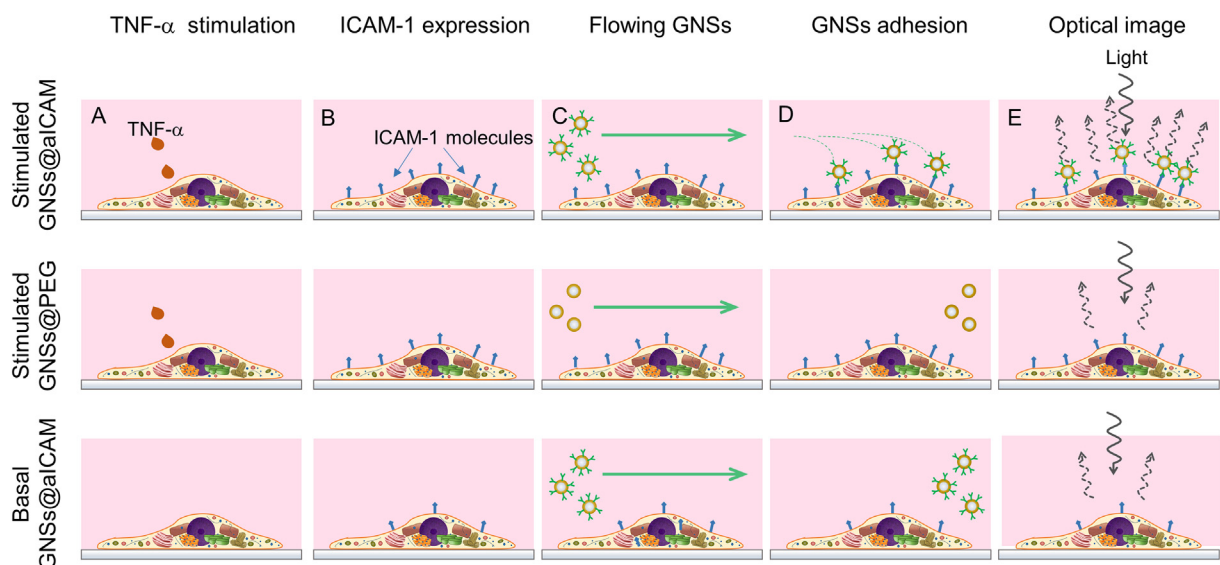


Figure 6. Step-by-step schematic description of the processes involved in the dynamic adhesion cellular imaging experiments.

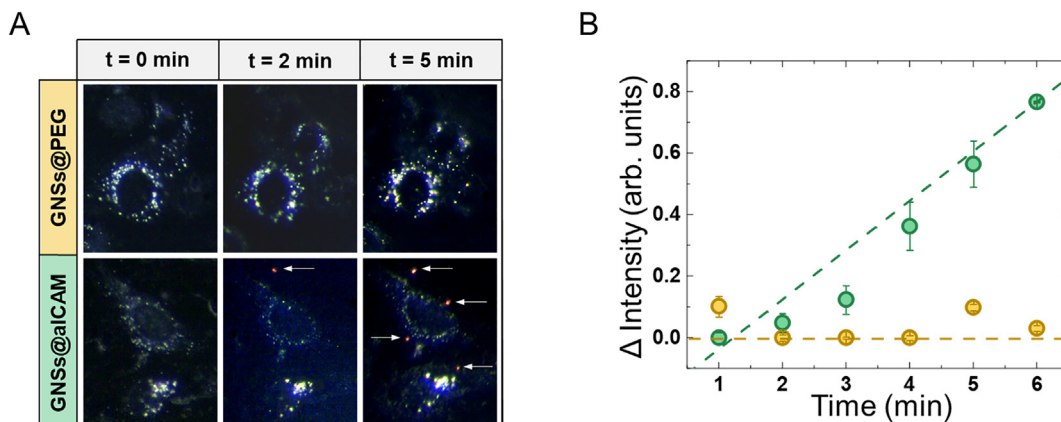


Figure 7. (A) DFM images of activated HMEC cells for different circulation times of GNSs@ PEG and GNSs@αICAM dispersions over activated cells with a shear stress of 1.7 dyn cm^{-2} . GNSs are remarked with white arrows. (B) DFM Intensity increase due to GNSs as a function of circulation time (5 min + 1 min of washing with PBS).

difference can be qualitatively explained by considering that, even in the basal state, cells overexpress a non-negligible number of ICAM-1 molecules (see Figure 3). Thus, after 1 h of static incubation, the nanoparticle-cell interaction time is high enough so that the expressed ICAM-1 molecules in the basal cells are almost saturated by functionalized (GNSs@αICAM) nanoparticles. This explains the substantial increase in the scattering (DFM and OCT) signal of GNSs@αICAM in respect to that of GNSs @ PEG for the basal state (see for instance Figure 4, B). This saturation of the ICAM molecules by functionalized nanoparticles in the basal state would explain also the slight increase measured in the scattered signal of these nanoparticles in the activated state (about 20%) and so the low adhesion efficiency obtained under static incubation. At variance, in the dynamic experiments the cell-nanoparticle interaction times are so short that the number of functionalized nanoparticles attached to cells is low and does not saturate the available ICAM sites either in the basal or in the activated cells states. This explains the larger adhesion efficiencies obtained under dynamical conditions as well as the decrease measured in

this efficiency with the increasing shear stress. Nevertheless, future experiments are underway to study the effect of the incubation time and/or the GNSs concentration to find out the optimal conditions maximizing the adhesion efficiency under static incubation conditions.

Conclusion

In this work we systematically evaluated the potential of gold nanoshells (GNSs) to act as molecular contrast agents for the early diagnose of atherosclerosis by optical coherence tomography (OCT). After proper functionalization with the cLABEL peptide, GNSs have proven to bind specifically to the ICAM-1 molecules overexpressed by TNF-α activated HMEC cells after static incubation. This specificity has been demonstrated by both dark field microscopy and OCT imaging modalities. The ability of the functionalized GNSs to attach to inflamed cells was also tested under dynamic conditions. Results indicate that even in these conditions the adhesion efficiency is higher than 30% and so

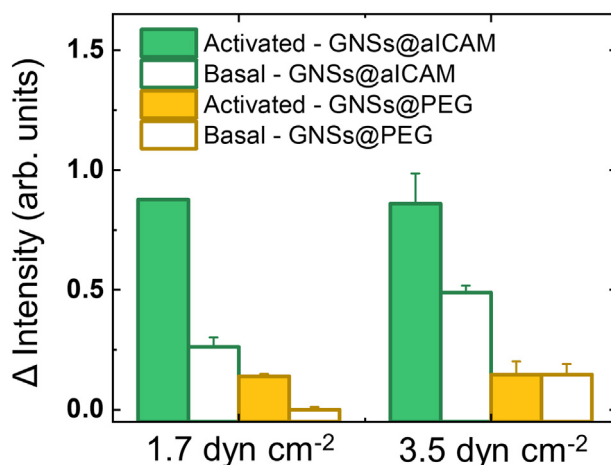


Figure 8. DFM intensity increase due to GNSs for two shear stresses (after 5 min flow plus 1 min of clearance with PBS).

pointing to the possibility of employing these nanoparticles in clinical OCT procedures. This work constitutes a first demonstration in vitro of the prowess of GNSs as molecular contrast agents to detect atherosclerosis in its first stages by CV-OCT. Thus, further efforts will be carried out in the near future to translate this system to ex vivo and in vivo models of inflammation targeting.

CRediT author statement

Tamara Muñoz-Ortiz: Formal analysis, Investigation, Writing – original draft preparation.

Jie Hu: Investigation, Writing – reviewing & editing.

Francisco Sanz-Rodríguez: Investigation.

Dirk H. Ortgies: Investigation, Writing – reviewing & editing.

Daniel Jaque: Funding acquisition, Writing – reviewing & editing.

Diego Méndez-González: Investigation, Writing – reviewing & editing.

Río Aguilar: Conceptualization, Writing – reviewing & editing.

Fernando Alfonso: Funding acquisition, Conceptualization, Writing – reviewing & editing.

Fernando Rivero: Funding acquisition, Conceptualization, Writing – reviewing & editing.

Emma Martín Rodríguez: Validation, Supervision, Writing – reviewing & editing.

José García Solé: Conceptualization, Supervision, Writing – original draft preparation.

Appendix A. Supplementary data

Supplementary data to this article can be found online at <https://doi.org/10.1016/j.nano.2022.102556>.

References

- Hansson GK. Inflammation, atherosclerosis, and coronary artery disease. *N Engl J Med* 2005;**352**:1685-95.
- Hu J, Ortgies DH, Martín Rodríguez E, Rivero F, Aguilar Torres R, Alfonso F, et al. Optical nanoparticles for cardiovascular imaging. *Adv Opt Mater* 2018;**6**:1800626.
- Douma K, Prinzen L, Slaaf DW, Reutelingsperger CPM, Biessen EAL, Hackeng TM, et al. Nanoparticles for optical molecular imaging of atherosclerosis. *Small* 2009;**5**:544-57.
- Sanz J, Fayad ZA. Imaging of atherosclerotic cardiovascular disease. *Nature* 2008;**451**:953-7.
- Khodabandehlou K, Masehi-Lano JJ, Poon C, Wang J, Chung EJ. Targeting cell adhesion molecules with nanoparticles using in vivo and flow-based in vitro models of atherosclerosis. *Exp Biol Med* 2017;**242**:799-812.
- McAteer MA, Choudhury RP. Targeted molecular imaging of vascular inflammation in cardiovascular disease using nano- and micro-sized agents. *Vasc Pharmacol* 2013;**58**:31-8.
- Otsuka F, Joner M, Prati F, Virmani R, Narula J. Clinical classification of plaque morphology in coronary disease. *Nat Rev Cardiol* 2014;**11**:379-89.
- Mizukoshi M, Kubo T, Takarada S, Kitabata H, Ino Y, Tanimoto T, et al. Coronary superficial and spotty calcium deposits in culprit coronary lesions of acute coronary syndrome as determined by optical coherence tomography. *Am J Cardiol* 2013;**112**:34-40.
- Aumann S, Donner S, Fischer J, Müller F. Optical coherence tomography (OCT): principle and technical realization. In: Bille JF, editor. *High resolution imaging in microscopy and ophthalmology*. Cham: Springer; 2019.
- Fercher AF, Drexler W, Hitzenberger CK, Lasser T. Optical coherence tomography — principles and applications. *Rep Prog Phys* 2003;**66**:239-303.
- Jefferson A, Wijesurendra RS, McAteer MA, Digby JE, Douglas G, Bannister T, et al. Molecular imaging with optical coherence tomography using ligand-conjugated microparticles that detect activated endothelial cells: rational design through target quantification. *Atherosclerosis* 2011;**219**:579-87.
- Hu J, Ortgies DH, Aguiar Torres R, Fernández N, Porto L, Martín Rodríguez E, et al. Quantum dots emitting in the third biological window as bimodal contrast agents for cardiovascular imaging. *Adv Funct Mater* 2017;**27**:1703276.
- Smith BR, Gambhir SS. Nanomaterials for in vivo imaging. *Chem Rev* 2017;**117**:901-86.
- Hu J, Gorsak T, Martín Rodríguez E, Calle D, Muñoz-Ortiz T, Jaque D, et al. Magnetic nanoplatelets for high contrast cardiovascular imaging by magnetically modulated optical coherence tomography. *ChemPhotoChem* 2019;**3**:529-39.
- Hu J, Rivero F, Torres RA, Loro Ramírez H, Rodríguez EM, Alfonso F, et al. Dynamic single gold nanoparticle visualization by clinical intracoronary optical coherence tomography. *J Biophotonics* 2017;**10**:674-82.
- Hu J, Abujetas DR, Tsoutsis D, Leggio L, Rivero F, Rodríguez EM, et al. Experimental evaluation of gold nanoparticles as infrared scatterers for advanced cardiovascular optical imaging. *APL Photonics* 2018;**3**:080803.
- Agrawal A, Huang S, Lin A, Lee M-H, Barton J, Drezek R, et al. Quantitative evaluation of optical coherence tomography signal enhancement with gold nanoshells. *J Biomed Opt* 2006;**11**:041121.
- Hu J, Sanz-Rodríguez F, Rivero F, Rodríguez EM, Torres RA, Ortgies DH, et al. Gold nanoshells: contrast agents for cell imaging by cardiovascular optical coherence tomography. *Nano Res* 2018;**11**:676-85.
- Wu JC, Bengel FM, Gambhir SS. Cardiovascular molecular imaging. *Radiology* 2007;**244**:337-55.
- Douglas G, Channon KM. The pathogenesis of atherosclerosis. *Medicine* 2014;**42**:480-4.
- Libby P. Inflammation in atherosclerosis. *Nature* 2002;**420**:868-74.
- Mestas J, Ley K. Monocyte-endothelial cell interactions in the development of atherosclerosis. *Trends Cardiovasc Med* 2008;**18**:228-32.
- Choudhury RP, Fisher EA. Molecular imaging in atherosclerosis, thrombosis, and vascular inflammation. *Arterioscler Thromb Vasc Biol* 2009;**29**:983-91.
- Gimbrone Jr MA, García-Cardeña G. Endothelial cell dysfunction and the pathobiology of atherosclerosis. *Circ Res* 2016;**118**:620-36.
- Watanabe T, Fan J. Atherosclerosis and inflammation mononuclear cell recruitment and adhesion molecules with reference to the implication of ICAM-1/LFA-1 pathway in atherogenesis. *Int J Cardiol* 1998;**66**:S45-53 discussion S5.
- Xu CR, Yusuf-Makagiansar H, Hu Y, Jois SDS, Siahaan TJ. Structural and ICAM-1-docking properties of a cyclic peptide from the I-domain of LFA-1: an inhibitor of ICAM-1/LFA-1-mediated T-cell adhesion. *J Biomol Struct Dyn* 2002;**19**:789-99.
- Zhang N, Chittasupho C, Duangrat C, Siahaan TJ, Berkland C. PLGA nanoparticle-peptide conjugate effectively targets intercellular cell-adhesion molecule-1. *Bioconjug Chem* 2008;**19**:145-52.
- Wong AK, Llanos P, Boroda N, Rosenberg SR, Rabbany SY. A parallel-plate flow chamber for mechanical characterization of endothelial cells exposed to laminar shear stress. *Cell Mol Bioeng* 2016;**9**:127-38.